Cement and Concrete Research 100 (2017) 263–274

Contents lists available at ScienceDirect

Cement and Concrete Research

journal homepage: www.elsevier.com/locate/cemconres

Numerical flow simulation of fresh concrete with viscous granular material model and smoothed particle hydrodynamics

Guodong Cao[a], Zhuguo Li[b,*]

[a] Graduate School of Science and Engineering, Yamaguchi University, Ube, Yamaguchi, Japan
[b] Graduate School of Science and Technology for Innovation, Yamaguchi University, Ube, Yamaguchi, Japan

ARTICLE INFO

Keywords:
Fresh concrete
Granular characteristic
Shearing time-dependence
Viscous granular material (VGM) model
Smoothed particle hydrodynamics (SPH)
L-flow test

ABSTRACT

The goal of this paper is to develop a numerical approach for fresh concrete's flow, by using the mesh free method, called Smoothed Particle Hydrodynamics (SPH), and a new rheological model named VGM (viscous granular material) model, which can describe the nonlinear, shearing time-dependent, and pressure-dependent characteristics of the flow behaviors of fresh concrete. Moreover, the visco-plastic model proposed by Murata was adopted to treat the slippage resistance of fresh concrete at its flow boundary. Next, the flow behaviors of fresh mortar in the L-flow test were observed experimentally and simulated numerically. As a result, it was found that VGM model is more accurate than Bingham model for simulating the flow of low fluidity mixture, since the former can reflect the change of internal structure of fresh concrete during the flow process.

1. Introduction

The concrete pump is widely used to transport concrete in construction site, and maximum pumping distance and height become greater and greater as high-rise buildings increase. Amount of reinforcing steel bars in concrete members has been increased for achieving earthquake-resistant structure. The use of various admixtures results in the diversity of fresh concrete's properties. Therefore, proper workability is required for fresh concrete, and it becomes difficult to judge the workability by the slump test or slump flow test. So far, a lot of studies on the rheological test method [1,2] have been performed to try to evaluate the flow ability of fresh concrete, but since the workability is not only dependent on flow ability, but also related with the structural, construction and environmental conditions, the workability would not be properly judged if only based on the rheological test results. There are no doubts that designing workability of concrete by experiment is costly and labor intensive. Therefore, it is a good alternative to evaluate and design the workability of fresh concrete based on numerical simulation [3–5].

At present, Bingham model is generally used to describe the rheological behavior of fresh concrete. Almost all the rheological tests are designed to measure the two parameters: yield stress and plastic viscosity of Bingham model to evaluate the consistency of fresh concrete [1]. And Bingham model is commonly used as a constitutive model of fresh concrete in numerical simulation [4,5]. High fluidity concrete has a fluid characteristic, and thus its flow behaviors are usually described approximately by Bingham model [6]. However, since fresh concrete is composed of cement and aggregate particles with inter-friction, and its deformation is time-dependent, it has the characteristics of both granular material and viscous material. Hence, fresh concrete is exactly a kind of viscous granular material rather than a viscous fluid, it is impossible that all the particles suspend in the mixing water without any contact [7].

Particle contact results in inter-particle friction. The inter-particle frictional resistance is dependent on the vertical pressure or normal stress on the shear plane. Hence, the deformation resistance of fresh concrete is pressure-dependent [7,8]. On the other hand, the particle arrangement, i.e. the structure of granular body, which is usually described by the distribution and mean value of particle contact angles, also affects the deformation resistance of fresh concrete, while mean particle contact angle changes with the deformation so that dilatancy occurs [9]. The existence of particle contact angle amplifies the pressure-dependence of the deformation resistance. Once the dilatant deformation is restrained, normal stress and accordingly deformation resistance increase [10]. Fresh concrete is essentially a kind of particle material that contains water. The physical flocculation, dispersion and hydration of cement particles cause the change in the particle arrangement of fresh concrete. It is considered that the change of fresh concrete's particle arrangement, during the rheological tests, results in that the flow curve of fresh concrete is nonlinear [6,11], and shearing time-dependent [12]. Due to the same reason, measuring value of yield stress varies with the shearing time [13].

* Corresponding author.
E-mail address: li@yamaguchi-u.ac.jp (Z. Li).

http://dx.doi.org/10.1016/j.cemconres.2017.07.005
Received 2 March 2017; Received in revised form 24 July 2017; Accepted 25 July 2017

Obviously, Bingham model is unable to describe the nonlinear, and normal stress-dependent characteristics of fresh concrete's flow behaviors, and it can't describe the change of rheological property with rest time and shearing time, i.e. the time-dependence of rheological property. The Herschel-Bulkley model, which is polynomial and quadratic function, was proposed to describe the nonlinear characteristic [14,15], but other characteristics are not expressed and the parameters in the model are lack of physical meanings and test methods [16].

Based on the assumption that yield stress and plastic viscosity increase with normal stress, a pressure-dependent model was proposed by Mori [8]. Roussel proposed a thixotropic model to describe the time-dependence of yield stress [13]. However, these improved Bingham model can't describe simultaneously the nonlinear characteristic, time-dependence, and pressure-dependence, and some of the parameters in the models can't be measured at present.

The Smoothed Particle Hydrodynamics (SPH) is a mesh free lagrangian method. It is applied to various flow problems with free surface [17,18]. As stated above, fresh concrete is a particle material. Particle-based numerical techniques are appropriate for simulating the flow behaviors of fresh concrete. Deeb used the SPH to simulate the slump flow tests of self-compacting concrete (SCC) with or without steel fibers [4]. And Badry proposed a SPH-based approach to estimate the yield stress and the distribution of coarse aggregates during the slump flow test of SCC [19]. Kulasegaram developed a numerical method with SPH to determine how the fibers distribute and orient themselves during the ultra-high performance SCC flows [20]. These numerical studies identified SPH's potential for numerical analysis of fresh concrete. However, these SPH methods have employed Bingham model or its improved form as a constitutive equation of fresh concrete, and didn't consider the slippage resistance from the flow boundaries.

As mentioned above, Bingham model may describe the relationship of shear stress and shear strain rate of high fluidity concrete, but can't describe nonlinear, time and pressure-dependent characteristics of rheological properties of ordinary fresh concrete. Recently, a new rheological model for fresh concrete, here briefly called VGM (viscous granular material) model, was proposed by Z. Li [21]. It contains two equations that describe respectively the deformation behavior under a shear stress before shear failure, and the flow resistance under a shear strain rate after shear failure. VGM model can express not only the nonlinear characteristic, but also the shearing time and pressure-dependent characteristics of rheological properties.

This paper aims to propose a numerical method for fresh concrete, based on SPH and VGM model. The slippage resistance is also taken into account at the flow boundaries. We firstly performed the L-flow tests of three mortar mixtures with different water-cement ratios (W/C), and recorded their flow situations by video camera. Then, we measured the parameters in the VGM model for the mortars with the rheometer developed by Z. Li [21]. Numerical simulations of the L-flow were finally conducted by using the SPH and the VGM model. Numerical analyses based on SPH and Bingham model were also done for the same mortars. The authors examined the difference between the numerical results based on the VGM model and Bingham model. The numerical results of VGM model based SPH simulation are more consistent with the experiment, since the yield stress and the plastic viscosity in VGM model change with shear deformation rather than constants.

2. SPH method

SPH method is a mesh free and particle-based method and originally used for continuum scale applications [22]. Besides the applications in astrophysics and solid problems such as dynamic material response [23], high velocity impact (HVI) [24] and explosion simulations [25], SPH method has also been applied to fluid problems, such as Newtonian and non-Newtonian flows with a free surface [18]. In SPH method, a system is represented by a set of discrete particles that possess material properties. Any particle i interacts with the others that are in a spherical domain, of which the radius (kH) is settled by a weight function or a smooth function [27], as shown in Fig. 1. The behaviors of discrete particles must obey the mechanical laws of motion, called governing equation.

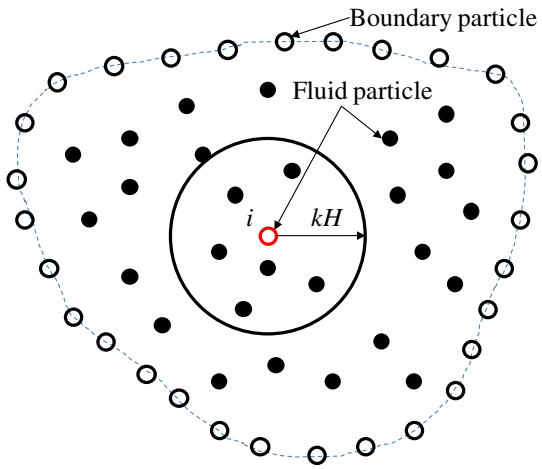

Fig. 1. Influential range of particle i in x and y directions.

2.1. Governing equation

The governing equations for granular material consist of the continuity and momentum equations. The continuity equation describes the mass conversation that particles' densities change with the corresponding deformation, while the momentum equation expresses the motion of particles. The mass and momentum conversation equations for a continuum are as follows.

$$\frac{d\rho}{dt} = -\rho\nabla\cdot v \tag{1}$$

$$\frac{dv}{dt} = \frac{1}{\rho}\nabla\cdot P + g \tag{2}$$

where, ρ is density of particle, v is velocity of particle, t is time, g is gravitational acceleration.

Also, the total stress tensor P in Eq. (2) is expressed by

$$P = -pI + \tau \tag{3}$$

where p is hydrostatic pressure at equilibrium, I is unit matrix, τ is extra stress tensor.

2.2. SPH approximation of governing equations

Two steps are need for obtaining an SPH formulation. The first step is to build a function and/or its derivative in continuous form as integral representation. This step is usually termed as kernel approximation. The second step is usually referred to the particle approximation. In this step, the computational domain is firstly discretized by describing the domain with a set of initial distributions of the particles, which represents an initial state. After the discretization, field variables of a particle i are approximated by a summation of the values of the particles in the influential range of the particle i. The integral of an arbitrary function $f(x)$ in the SPH is based on the kernel function W and is expressed by

$$f(x) \approx \int f(x')W(|x - x'|, H)dx' \tag{4}$$

where, H is smoothed length for defining the influential range of kernel function. The kernel function W is usually chosen to be an even function, and should satisfy the conditions, such as the normalization condition (see Eq. (5)) and the compact condition (see Eq. (6)).

$$\int_{\Omega} W(|x-x'|,H)dx' = 1 \tag{5}$$

$$W(|x-x'|,H) = 0, \quad x-x' > kH \tag{6}$$

where, k is a parameter related to the smooth function. kH is effective radius of the smooth function (see Fig. 1). When H approaches to zero, the kernel function W need to be a delta function. After describing the computational domain with a finite number of particles, the continuous form of kernel approximation shown in Eq. (4) can be written as a discretized form of the summation of the influenced particles as follows.

$$f(x_i) = \sum_j \frac{m_j}{\rho_j} f(x_j) W(|x_i - x_j|, H) \tag{7}$$

In this study, we adopted the usually used cubic spine function as kernel function, as shown in the following:

$$W(r,H) = \alpha_d \begin{cases} 1 - \frac{3}{2}{q_H}^2 + \frac{3}{4}{q_H}^3 & 0 \le q_H \le 1 \\ \frac{1}{4}(2-q_H)^3 & 1 \le q_H \le 2 \\ 0 & q_H \ge 2 \end{cases} \tag{8}$$

where $r = (r_i - r_j)$, α_d is normalization factor and is equal to $10/7\pi H^2$ in case of two dimensions or $1/\pi H^3$ in case of three dimensions.

In SPH, the movements of all the discrete particles are calculated individually, and further accumulated to clarify the deformation and movement of whole system. Hence, the governing equations need to be discretized for each discrete particle. In this study, we used the most popular SPH approximation forms to discretize the governing equations. Discretized continuity and momentum equations are expressed by Eqs. (9), and (10), respectively [17]. They were used to calculate the local density, velocity and acceleration of each particle.

$$\frac{d\rho_i}{dt} = \sum_j m_j (v_i - v_j) \nabla_i W_{ij} \tag{9}$$

$$\frac{dv_i}{dt} = \sum_j m_j \left(\frac{P_i}{\rho_i^2} + \frac{P_j}{\rho_j^2} \right) \nabla_i W_{ij} + g \tag{10}$$

2.3. Equation of state

An equation of state must be used to describe the relationship between pressures and densities of the particles. Fluid is generally incompressible. However, since the incompressible SPH method (ISPH), using the actual equation of state (Pressure Poisson Equation), needs extremely small time step, the solving process is greatly slowed. Hence, in most cases, fluid is treated to be weakly compressible to the advantage of shortening the solving process, called weakly compressible SPH method (WCSPH) here.

Fresh concrete contains tiny air bubbles. Some of them would get out while fresh concrete flows. It is reasonable to consider that fresh concrete has weak compressibility. Shadloo compared the ISPH and the WCSPH, and concluded that the WCSPH can give an accurate and reliable analysis like as the ISPH method does [26]. Thus, we used the WCSPH method in this study, the following thermodynamic equation of state was employed according to Reference [27].

$$P = B\left[\left(\frac{\rho}{\rho_0} \right)^a - 1 \right] \tag{11}$$

where, $B = {c_0}^2 \rho_0 / a$, $a = 7$, and c_0 is sound speed under the initial density ρ_o.

2.4. Artificial viscosity

In the SPH method, when the particles are in a tension state, their motions become unstable. As a consequence, the particles tend to clump together and show unrealistic physical behavior. In order to stabilize the numerical scheme and to alleviate the unphysical oscillations, the artificial viscosity approach was adopted in this study, which is expressed by Eq. (12) [28].

$$\prod_{ij} = \begin{cases} \frac{-\alpha \bar{c}_{ij}}{\bar{\rho}_{ij}} \cdot \frac{h v_{ij} r_{ij}}{r_{ij}^2 + 0.01H^2} & v_{ij} r_{ij} < 0 \\ 0 & v_{ij} r_{ij} > 0 \end{cases} \tag{12}$$

where, α is a free parameter changing with numerical problem, $\bar{c}_{ij} = (c_i + c_j)/2$, $\bar{\rho}_{ij} = (\rho_i + \rho_j)/2$. $v_{ij} = (v_i - v_j)$ is relative velocity of particles i and j, and $r_{ij} = (r_i - r_j)$ is relative distance of particles i and j.

2.5. Constitutive equation

2.5.1. Bingham model

Present SPH simulations of fresh concrete have generally used Bingham model as constitutive model, as shown in Eq. (13).

$$\tau = \left(\eta_b + \frac{\tau_0}{\dot{\gamma}} \right) \dot{\gamma} \tag{13}$$

where, τ_0 is yield stress, η_b is plastic viscosity, $\dot{\gamma}$ is shear strain rate.

The stress tensor and the shear strain rate tensor are written as

$$\tau = \sqrt{\frac{1}{2}\tau_{ij}\tau_{ij}}, \ \dot{\gamma} = \sqrt{\frac{1}{2}\dot{\gamma}_{ij}\dot{\gamma}_{ij}} \tag{14}$$

The constitutive law shown in Eq. (13) is discontinuity when shear stress τ approaches to the yield stress τ_0. When subjected to the τ_0, the apparent viscosity ($\eta_{app} = \tau/\dot{\gamma}$) becomes infinite so that numerical divergence occurs in the computation. Hence, it is difficult to introduce directly Bingham model into the SPH simulation. A regularized Bingham model, as shown in Fig. 1(a) and in Eq. (15), is usually used in SPH simulations of fresh concrete [29]. In this study, we first used the regularized Bingham model to do SPH simulations.

$$\tau = \left(\eta_b + \tau_0 \frac{[1 - e^{\beta\dot{\gamma}}]}{\dot{\gamma}} \right) \dot{\gamma} \tag{15}$$

where, β is a parameter related to the transition between the solid and fluid regimes. The larger the β, the sharper the transition [30].

2.5.2. VGM model

As stated above, Bingham model can't exactly describe various rheological behaviors of fresh concrete overall since fresh concrete has granular characteristic. For this reason, Li proposed the VGM model based on a series of theoretical analyses [6,31] and experimental investigations [32,33], as shown in Eqs. (16) and (17) [21,31]. It was verified that this model is able to describe various rheological characteristics of fresh concrete [34]. When shear stress (τ) and shear strain (γ) are smaller than the shear failure limit stress (τ_f) and limit strain (γ_f), fresh concrete is in visco-elasto-plastic state, and the shear strain γ under a shear stress τ is expressed by Eq. (16). When $\tau \ge \tau_f$ and $\gamma \ge \gamma_f$, fresh concrete enters into the shear failure state, the $\tau - \gamma$ relationship is described by Eq. (17).

if $\tau < \tau_f, \ \gamma < \gamma_f$

$$\gamma = \frac{c_6 \tau}{c_2 + c_3 \tau} \cdot \frac{1}{\sigma_n + C_{w2}} \cdot [1 - \exp(-q t)] = \gamma_\infty \cdot [1 - \exp(-q t)]$$

$$\dot{\gamma} = \frac{c_2 c_6 s_1 / (\sigma_n + C_{w2})}{(c_2 + c_3 \tau)^2} \cdot \left[1 - \exp\left(-q \frac{\tau}{s_1} \right) \right] + \frac{c_7 \tau (c_2 + c_3 \tau)}{\exp(q\tau / s_1)}$$

$$c_2 = \varphi + \theta_0, \ c_3 = \frac{\theta_f - \theta_0}{\tau_f}, \ c_6 = \frac{1}{2} N \Lambda_0$$

$$q = c_8 (\sigma_n + C_{w2}) \left(\frac{c_2 + c_3 \tau}{c_6} \right)^2, \ C_{w2} = N f_{wm} \cos\theta_0$$

$$\gamma_\infty = \frac{c_6 \tau}{c_2 + c_3 \tau} \cdot \frac{1}{\sigma_n + C_{w2}}, \ c_8 = \frac{2 \Lambda_c c_6^2}{h N c_2 \exp(E/kT)} \tag{16}$$

$$\text{if } \tau \geq \tau_f,\ \gamma \geq \gamma_f$$

$$\tau = \sigma_n \tan(\theta_f e^{-\kappa\cdot\dot{\gamma}\cdot(t-t_f)} + \varphi) + C_{w1} + \frac{\eta}{\cos(\theta_f e^{-\kappa\cdot\dot{\gamma}\cdot(t-t_f)})}\dot{\gamma}$$

$$= \tau_f^* + \eta_t\dot{\gamma}$$

$$\tau_f^* = \sigma_n \tan(\theta_f e^{-\kappa\cdot\dot{\gamma}\cdot(t-t_f)} + \varphi) + C_{w1},\quad \eta_t = \frac{\eta}{\cos(\theta_f e^{-\kappa\cdot\dot{\gamma}\cdot(t-t_f)})} \tag{17}$$

where, σ_n is normal stress acting on the shear plane, N is amount of particle contacts on unit area of the shear plane, κ is a parameter related to shearing time-dependence, t_f is shearing time before shear failure, s_1 is loading speed in case of stress growth control, θ_0, θ_f is average particle contact angle at the initial state, and the shear failure point, respectively, Λ_0, Λ_c is average moving distance of all particles in the beginning, and average moving distance of cement particles for overcoming potential barrier, respectively, E is mean potential energy barrier of cement particles that results in a viscous resistance, T is absolute temperature, h is Planck constant, ϕ is average inter-particle frictional angle, C_{w1}, C_{w2}, f_{wm} is shear resistance, vertical stress, and adhesive force caused by the surface tension and suction of mixing water, respectively, η is the essential viscosity that is associated with temperature and potential energy of cement particles when there is no particle contact in fresh concrete.

The shear failure limit stress τ_f is mainly dependent on normal stress σ_n, mean particle contact angle θ_f, and mean inter-particle frictional angle ϕ, and is expressed by Eq. (18) [21].

$$\tau_f = \sigma_n \tan(\theta_f + \varphi) + C_{w1} \tag{18}$$

Because almost all the present rheometers of fresh concrete adopt the rotational speed sweep control method, it is impossible to evaluate the deformation behavior of fresh concrete before yield. VMG model not only describes the flow behaviors of fresh concrete in shear failure state, i.e. in yielded state, but also provides the information about the deformation before yield.

Eq. (17) contains the parameters of ϕ and σ_n so that VGM model can reflect the granular and pressure-dependent characteristics of fresh concrete. Moreover, the term $\theta_f \exp.[-\kappa\cdot\dot{\gamma}\cdot(t-t_f)]$ in the Eq. (17) expresses actually the change of mean particle contact angle with shearing time, i.e. reflects the change in the flocculent or interlocking structure of particles, when fresh concrete deforms or flows. If rewriting Eq. (17) in the form of Bingham equation, yield stress τ_f^* and plastic viscosity η_t of VGM model are not constants, varying with shear rate $\dot{\gamma}$ and shearing time t. Hence, VGM model can describe the non-linear and shearing time-dependent characteristics of fresh concrete's rheological behaviors.

The relationships between shear stress and shear strain rate, expressed by Eqs. (16) and (17), are shown in Fig. 2(b). The whole flow curve consists of three parts. In the first part I, the particle contacts are loose, thus whole system is easy to deform, and the shear strain rate increases with shear stress. However, because the particles have to move to the positions with higher resistance for matching with subjected external force, the particle contacts become denser and denser with deformation, thus the shear strain rate begins to decrease at a certain shear stress even shear stress is increased (see Part II in Fig. 2(b)). There is a limit in the increase of particle interlocking. If shear stress is increased continually and exceeds the stress limit τ_f of shear failure, the interlocking structure will be broken, the system enters into the shear failure state, and thus the shear strain rate increases with shear stress again (see Part III in Fig. 2(b)). At the shear failure point, the average particle contact angle (θ) reaches to the maximum value θ_f, but decreases with the increase of the shear deformation in the shear failure state. Also, at the shear failure point, the shear strain rate $\dot{\gamma}_f$ is very small, nearly approaches to zero.

In order to properly simulate the flow of fresh concrete under various conditions, in this study we incorporated VGM model into the SPH program as constitutive model. For a detailed clarification of material's properties, the description of the deformation behavior before the shear failure, shown in Eq. (16), is of great significance, and if using Eq. (16) as a constitutive equation before yield, the divergence problem in the numerical analysis mentioned above can be avoided. However, Eq. (16) describes the deforming behavior of fresh concrete before yield. A precise calculation of the shear deformation before yield is not necessary for simulating the flow of fresh concrete during pumping or casting. And, because Eq. (16) is nonlinear function, it is extremely difficult to apply directly this complicated equation in the numerical simulation. Therefore, we simplified the flow curve before yield with a straight line, as shown in Fig. 2(c). Because the $\dot{\gamma}_f$ is very small, the slope ($\tau_f/\dot{\gamma}_f$) of the line is large, i.e. the viscosity before yield is extremely large. Similar simplification is also found in Reference [35].

$$\tau = \frac{\tau_f}{\dot{\gamma}_f}\dot{\gamma} \qquad (\text{if } \tau < \tau_f) \tag{19}$$

where $\dot{\gamma}_f$ is the shear strain rate at the shear failure point.

2.6. Boundary condition

Two types of boundary conditions need to be taken into account. Firstly, when a particle approaches boundary, the kernel function will be truncated and unphysical penetration will happen. This problem further reduces the accuracy of SPH method. For solving the problem, in this work we employed the repulsive boundary condition developed by Monaghan [28]. Secondly, the discrete particles of fresh concrete may slip at the boundary and thus suffer from slippage resistance. In most case, coarse aggregates are surrounded by mortar matrix. Therefore, it is almost mortar matrix at boundary. The slippage resistance has important effect on flow process of fresh concrete (see Section 4.2). We used the visco-plastic model of fresh mortar matrix to describe the slippage resistance, which was proposed by Murata, as shown in Eq. (20) [36]

$$\tau_s = \eta_s v + \tau_{sy} \tag{20}$$

where, τ_s is slippage resistant stress at boundary, η_s is plastic viscosity of slippage, τ_{sy} is yield stress of slippage.

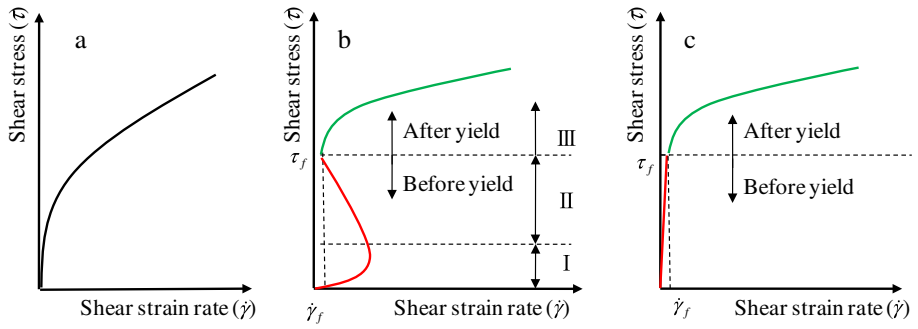

Fig. 2. The $\tau - \dot{\gamma}$ relationship: (a) Regularized Bingham model, (b) VGM model, and (c) simplified VGM model.

2.7. Integration scheme

Predictor-Corrector algorithm [37] was employed to execute the time integration. If considering the mass and momentum conversation equation (Eqs. (1) and (2)) in the form of $d\rho/d_t = S$, $d_v/d_t = F$, all the values of time-variant quantities are predicted at the time step n + 1, based on the time step n + 1/2 as follows:

$$\rho^{n+1/2} = \rho^n + \frac{\Delta t}{2}S^n, \quad v^{n+1/2} = v^n + \frac{\Delta t}{2}F^n \tag{21}$$

Then, these values are updated at another half time step.

$$\rho^{n+1/2} = \rho^n + \frac{\Delta t}{2}S^{n+1/2}, \quad v^{n+1/2} = v^n + \frac{\Delta t}{2}F^{n+1/2} \tag{22}$$

At the end of the time step, the values are calculated as follows:

$$\rho^{n+1} = 2\rho^{n+1/2} - \rho^n, \quad v^{n+1} = 2v^{n+1/2} - v^n \tag{23}$$

The selection of the magnitude of time step Δt is dependent on the Courant Friedrichs Lewy (CFL) condition, the force terms, and the viscous diffusion terms. Δt is expressed by Eq. (24) [37]

$$\Delta t = 0.3\ \min(\Delta t_f, \Delta t_{cv}) \tag{24}$$

$$\Delta t_f = \min(\sqrt{H/|f|}), \quad \Delta t_{cv} = \min(H/(c_s + \max\ |Hv_{ij}r_{ij}/r_{ij}^2|)) \tag{25}$$

where f is a force acting on per unit mass, c_s is a constant.

3. Experiment

For investigating the superiority of the SPH method incorporating the VGM model over the Bingham model, we compared the experimental and numerical results of the L-flow test of fresh mortar. Though the size distribution of aggregate particles in fresh mortar is different from fresh concrete, both of them are viscous granular material, and have similar internal structure and rheological characteristics. Moreover, if using fresh concrete, the precision and repeatability of experimental results decrease due to the random distribution of coarse aggregate particles, and in order to reduce the effect of coarser particles' segregation, three series of fresh mortar samples were used in our L-flow tests and SPH simulations.

3.1. L-flow test

The geometry of L-shaped box is shown in Fig. 3. A tapeline was stuck by instant glue on the inside of the L-box's bottom to measure the flowing distance of fresh mortar. The tapeline was 5 mm width and 1 mm thickness, and the scale interval was 0.5 mm. The vertical section of L-box has a capacity of 2.5 l. The sliding door was lifted up quickly within 2–3 s. After the door was opened, the flowing distances of the mortar sample were recorded at a certain time interval. The L-flow test was repeated three times for each mortar sample.

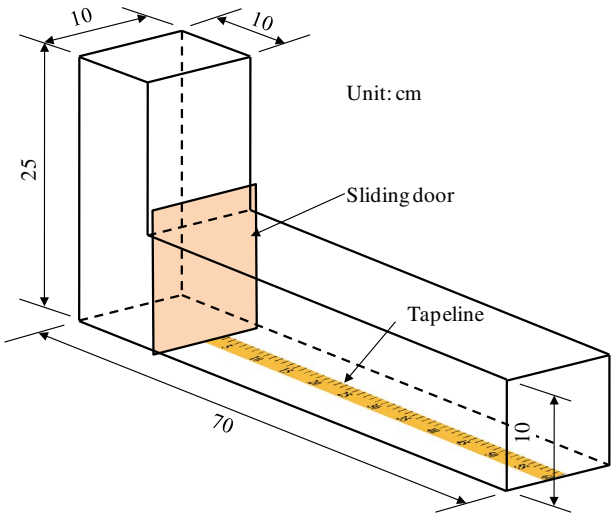

Fig. 3. Geometry of L-shaped box used in the L-flow test.

Table 1
Mix proportions of mortars and results of the flow table test.

No.	W/C	S/C	SP/C (%)	Unit mass (kg/m^3)				Spread diameter (mm)
				W	C	S	SP	
1	0.40	2	0.5	258.6	646.6	1293.2	3.2	168
2	0.45	2	0.5	281.5	625.4	1250.9	3.1	205
3	0.55	2	0.5	322.9	587.0	1174.0	2.9	208

Notes: *W*: water, *C*: ordinary Portland cement, *S*: sea sand, *W/C*: water-cement ratio, *S/C*: sand-cement ratio by mass, *SP*: high range water reducing and retarding admixture.

Mix proportions of three series of mortars are presented in Table 1. Ordinary Portland cement with specific surface area of 3500 cm^2/g and density of 3.16 g/cm^3 was used. Fine aggregate was sea sand with density of 2.57 g/cm^3 in saturated surface dry state, water absorption rate of 1.36%, solid volume percentage of 66.7%, and fineness modulus of 2.90, respectively. A compound admixture of high-range water reducer and retarder was used to increase the fluidity of the fresh mortars. Mass ratio of sand to cement and admixture dosage were kept to be 2.0, and 0.5%, respectively, but three series of mortars had different W/C.

The cement and sand were first put into the mixer bowl, and mixed at 48 rpm for 1 min. Then water and the admixture were added and further mixed at the same rotation speed for 2 min. After the mixing, the flow table test was performed according to JIS (Japan Industry Standard) R 5201: 2015. The spread diameters were measured, after the table was dropped through a height of 12.5 mm, 15 times in 15 s. The flow table tests were conducted three times for each mortar mixture, and the ranges of the spread diameters of series No.1–No.3 were 165–172, 201–208, and 207–210 mm, respectively. Their average values were shown in Table 1.

3.2. Measurement of input parameters

A rheometer shown in Fig. 4, called RSNS rheometer, was recently developed by Li for measuring the parameters of VGM model [21]. The RSNS rheometer has a motionless axis, thus fresh concrete or mortar sample is subjected to ring shear between two blades in radial pattern. Also, the RSNS rheometer can be operated by toque growth or rotation speed sweep control method, and the vertical pressure, acting on the shear plane, can be freely adjusted by two air cylinders. After mixing the mortars, we used the RSNS rheometer to measure the parameters in Eqs. (16) and (17). The thickness of sample is 100 mm, and the diameters of sample's periphery and inner circumference are 340 mm and 28 mm, respectively. The measurement was repeated three times for each mixture. The detailed measurement and calculation methods of the parameters can be found in Reference [21]. We also measured the Bingham model parameters (yield stress τ_0 and plastic viscosity η_b) of three series of mortars with the RSNS rheometer. The average of three measuring results of each parameter was shown in Table 2. The standard deviation of three measuring results of every parameter was less than 10%.

As shown in Eq. (18), the shear failure limit stress τ_f is dependent on the normal stress σ_n, Thus it should be noted that the τ_f shown in Table 2 was only a specific measuring value under the σ_n that is also shown in Table 2. For different σ_n, τ_f can be calculated by Eq. (18).

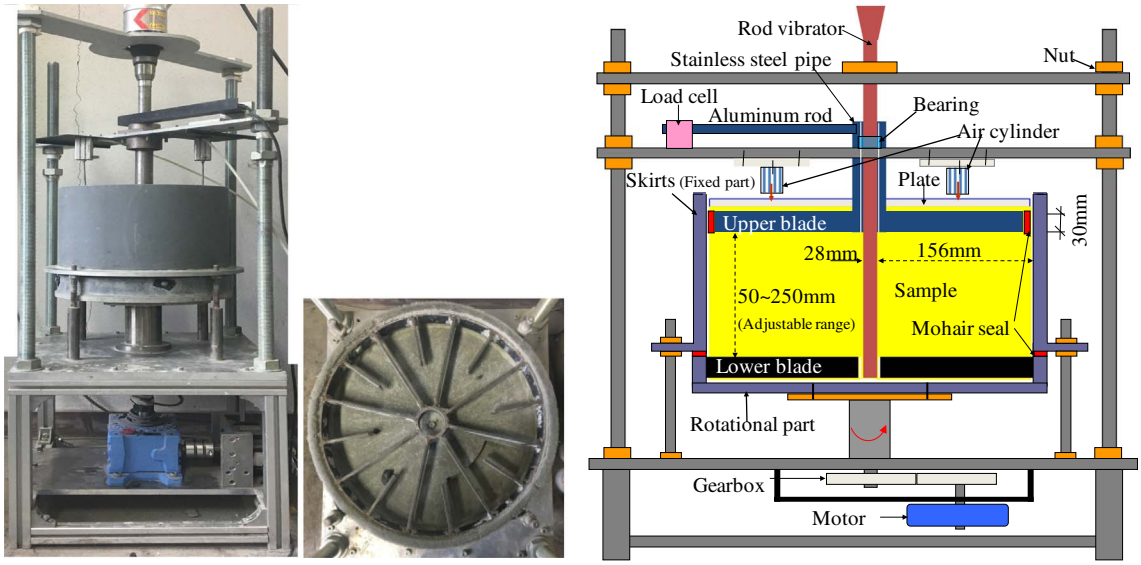

(a) apparatus (b) planform of lower blade (c) 2-D diagram

Fig. 4. RSNS rheometer.

4. Comparison of experimental and numerical results

4.1. Experimental results

Final flow shapes of the mortars in the L-flow box are shown in Fig. 5. The final flow distance of series No. 1 mortar was shortest. This is because No. 1 had the lowest W/C (0.40), and accordingly had the lowest fluidity (the spread diameter of the flow table test was only 168 mm). However, in case of series No. 3, it had the largest W/C (0.55) and the largest spread diameter (208 mm), almost all the samples flowed out the vertical section of the L-flow box, and the final shape was nearly horizontal. Variation of the L-flow distance with the elapsed time is shown in Fig. 6. The data in Fig. 6 were mean values of three times measurements for mortar mixtures. The flow speed of No. 3 was the fastest, compared to other two series. Although the final flow distances of series No. 2 and No. 3 were near (about 6 cm), but the former had a lower flow speed so that it spent more time till the flow stopped.

4.2. Numerical results and discussion

In the L-flow test, since normal stress σ_n varies with location, τ_f of samples at different locations are different. Hence, we firstly calculated the σ_n and further the τ_f at different locations. Then, the shear stress τ, acting on the sample at different locations, was calculated according to Eq. (14). The stress state (yield or not) of sample was judged by comparing the τ_f and τ. According to the stress state, we selected Eq. (17) or Eq. (19) to calculate the shear strain rate at every time step.

After yield, the τ_f^* and the η_t shown in Eq. (17) vary with shear rate $\dot{\gamma}$ and time t, they were calculated at step n (time interval Δt) on basis of step n-1, as shown in Eq. (26).

$$[\tau_f^*]^n = [\sigma_n]_n \tan(\theta_f e^{-\kappa\cdot[\dot{\gamma}]^{n-1}\cdot\Delta t} + \varphi) + C_{w1}$$
$$[\eta_t]^n = \frac{\eta}{\cos(\theta_f e^{-\kappa\cdot[\dot{\gamma}]^{n-1}\cdot\Delta t})} \quad (26)$$

In our SPH simulations, 2376 discrete particles were used to represent each of the fresh mortar. And the inner walls of the L-flow box and the sliding door were represented by 3234 fixed boundary particles, and 140 mobile boundary particles, respectively. In the beginning, the mobile boundary particles were let to move upward at a speed of 0.1 m/s, and they were stopped after they moved vertically 25 cm. The final flow shapes of three series of mortars obtained by the SPH method are shown in Fig. 7. Like the experimental results, the final flow distances increase with the decrease of W/C. In case of series No. 1 and No. 2, the final flow distance of VGM model is slightly larger than that of Bingham model.

Fig. 8 indicates the comparison of the relationships between the flow distance and the elapsed time, which are obtained by the experiments, and the SPH methods using the two models, respectively (when the flow velocity is less than 0.015 m/s, it is regarded that the flow stopped). As shown in this figure, for series No. 1 and No. 2, the numerical results using the VGM model are more consistent with the experimental results, the flow distance calculated by Bingham model is smaller than that obtained by the VGM model for the same time. The errors of the numerical results using VGM model to the experimental results are almost within the range of ± 12%. But when using Bingham model, the errors are − 20–22%. However, in case of series No. 3, the numerical results using either of the VGM and Bingham models are very close to the experimental results. The errors of the numerical results based on any of the two models are within ± 11%.

In order to clarify the effect of slippage resistance, the numerical

Table 2
The input parameters of numerical simulations.

Series no.	Parameters in VGM model								Bingham model parameters		Boundary model parameters	
	τ_f(Pa)	$\dot{\gamma}_f$(s^{-1})	η(Pa·s)	C_{w1}(Pa)	ϕ (rad)	θ_f (rad)	κ	σ_n (Pa)	τ_0 (Pa)	η_b(Pa·s)	τ_{sy} (Pa)	η_s (Pa·s)
1	1538	0.20	772	400	0.157	0.284	2.2	2412	1254	833	2.0	100
2	569	0.18	558	150	0.054	0.121	1.5	2372	379	560	1.0	40
3	302	0.16	455	90	0.030	0.062	0.7	2300	111	457	0.2	5

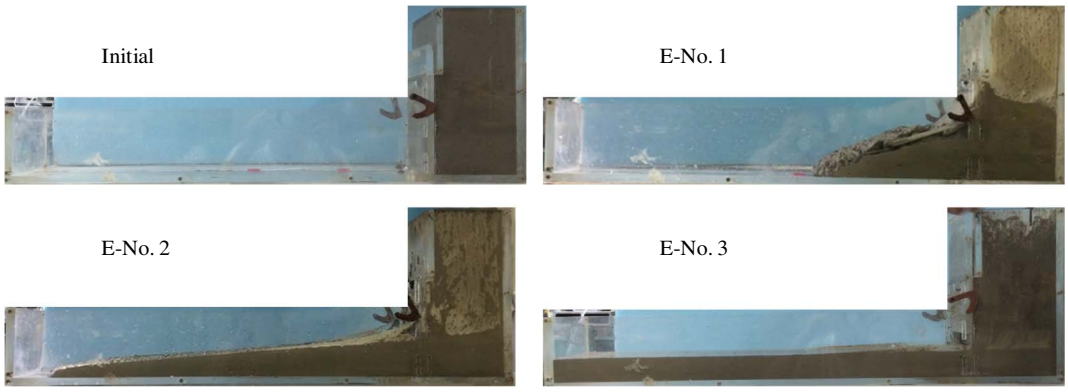

Fig. 5. Final shapes of fresh mortars in the L-flow box (E-No. n represents the experimental results of series No. n).

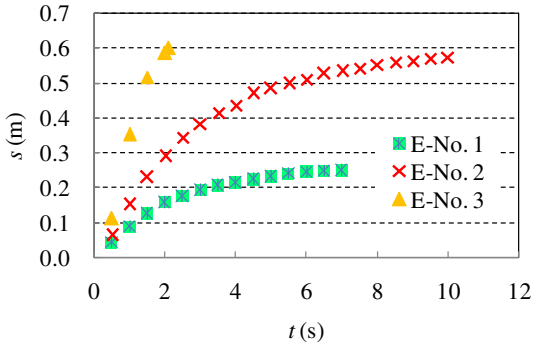

Fig. 6. Experimental results of the L-flow distance changing over time.

results without considering the slippage resistance were also shown in Fig. 8. The numerical results of series No. 3, using the VGM model but ignoring the slippage resistance, were close to experimental results. But for series No. 1 and No. 2, the numerical results were not well consistent with the experimental results when the slippage resistance was not taken into account. This is because that the slippage resistance increases with the decrease of fluidity. Hence, in case of series No.3 with a lower W/C, even if the slippage resistance was ignored, there was no great difference between the numerical and experimental results, but for series No.1 and No.2, the slippage resistance is needed to consider. It is also concluded that the visco-plastic model is apt to use in SPH approach of fresh concrete.

When the W/C is low, fresh mortar has a low fluidity so that its fluid or suspension characteristic becomes unobvious. The interaction between the particles or the particles' interlocking gives a prominent influence on the flow resistance of fresh mortar. The VGM model considers the change of fresh concrete's particle arrangement during the flow through introducing variable yield stress τ_f^* and plastic viscosity η_t, which vary with shearing time t, as shown in Eq. (17). As explained above, the particle arrangement of fresh concrete is expressed by the mean particle contact angle (θ), the variations of τ_f^* and η_t are basically

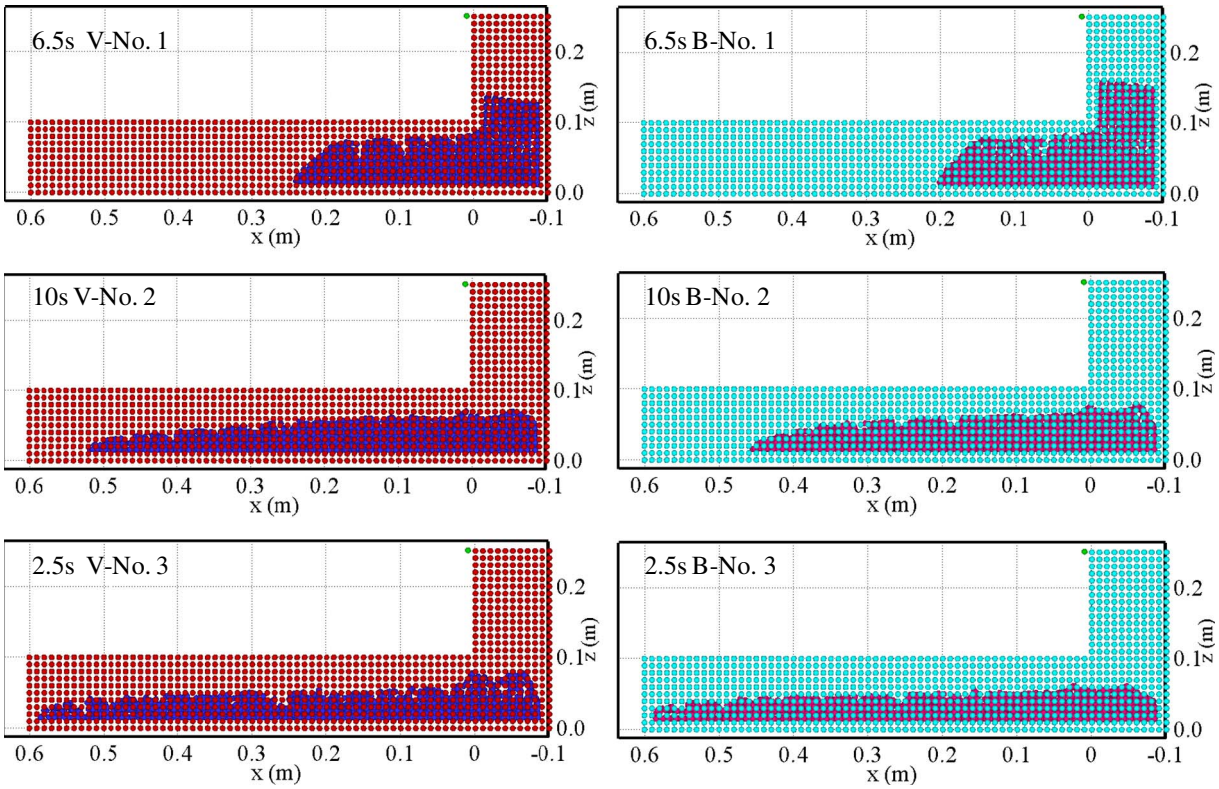

Fig. 7. Final shape of L-flow simulation. (V-No. n and B-No. n represent the numerical results using VGM model, and Bingham model, respectively).

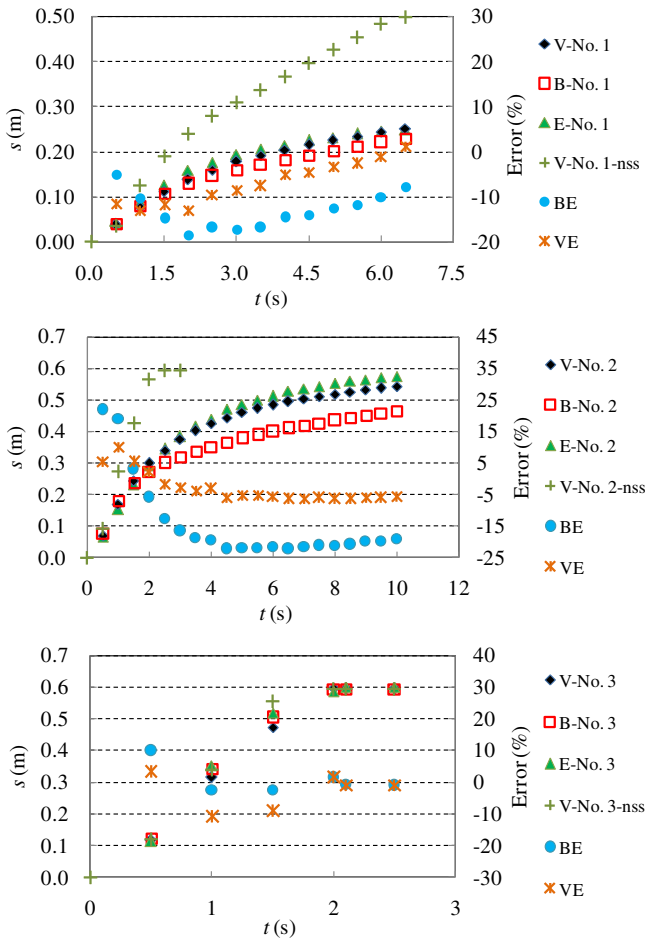

Fig. 8. Comparison of the numerical and experimental results of L-flow test. (VE, BE represent the error of numerical results based on VGM, and Bingham model, respectively, to experimental results, V-No. n-nss represents the numerical results using VGM model but not considering the slippage resistance).

resulted from the change of θ with shearing time. However, for the fresh mortar having high fluidity, its fluid characteristic is predominant, accordingly the effect of the particle arrangement becomes slight. Hence, in this case, the VGM model has no advantage over Bingham model in the numerical analysis.

Fig. 9 shows the relationship between the flow velocity and the flow time. The numerical results are close to the experimental results for three mixtures. The flow velocity decreases with the flow time for any of the mixtures. And the maximum flow velocity increases with the increase of W/C. This is because that the viscosity of mortar decreases with the increase of W/C.

Figs. 10 and 11 indicate the distributions of τ_f^* and η_t of the moving discrete particles of the mortar samples at the three moments, respectively. As seen from Figs. 10 and 11, the τ_f^* and η_t decrease with the increase of W/C. For the same sample and flow moment, the τ_f^* at lower location is larger. This is because the σ_n is larger at the lower location. Moreover, for the same flow moment, the discrete particles moving in the horizontal section of the box have smaller τ_f^* and η_t than that in the left vertical section. The τ_f^* of all the series and the η_t of series No.1 and No.2 decrease obviously with the flow time. But series No. 3 has a higher fluidity, thus its η_t is so small that it isn't almost further reduced by the free flow.

Fig. 12 shows the variations of the average values of τ_f^* and η_t of the whole moving particles after yield with the flow time. The average τ_f^* decreases with the flow time and finally approaches to a certain value. This is because the particle interlocking is reduced by the free flow. The decrease of normal stress σ_n is another reason, along with the samples moving from the vertical section to the horizontal section of the L-box. But after a long time flow, the particle interlocking approaches to the smallest degree or complete breakdown, and the σ_n at the horizontal section no longer decreases, the τ_f^* doesn't further change. The average η_t of series No.1 decreases with the flow time. However, the average η_t of any of series No.2 and No.3 nearly don't change. Series No.2 and No.3 had a larger.

W/C, accordingly had higher fluidity, the particle interlocking structure in initial state is so weak that it can't be further broken.

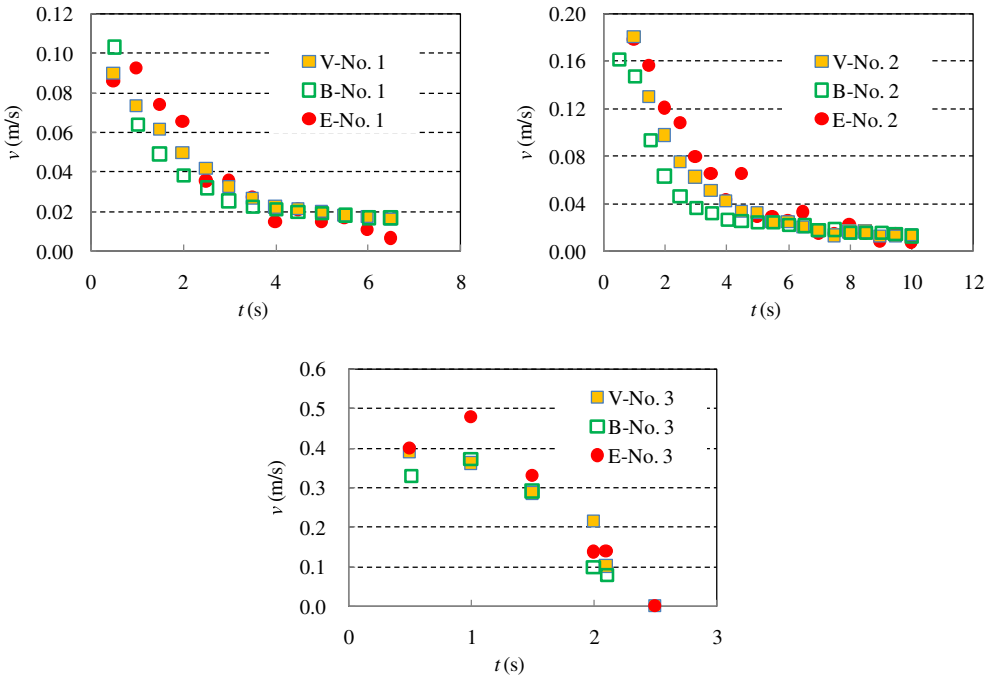

Fig. 9. Flow velocity of the mortars in L-flow box.

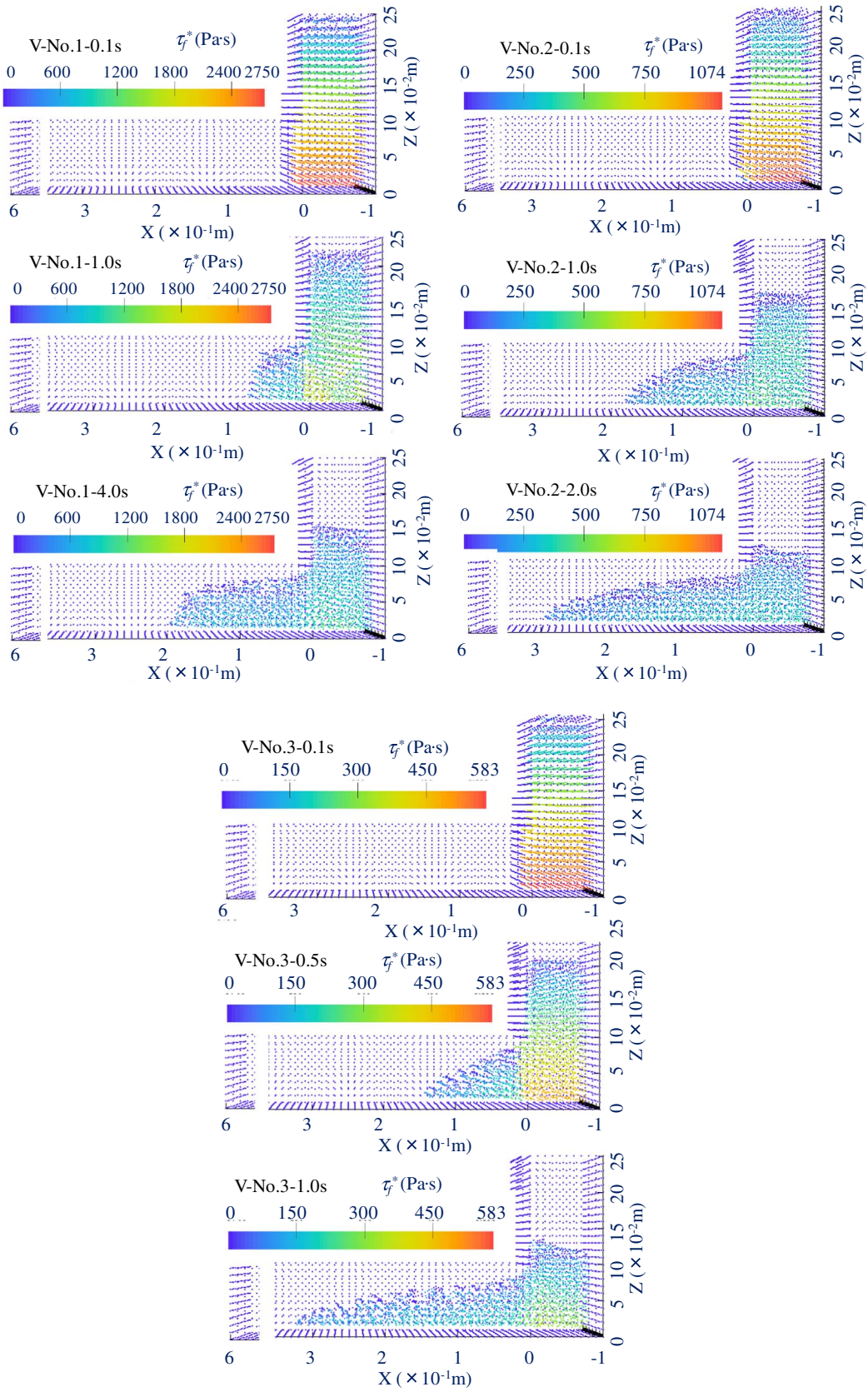

Fig. 10. Calculating results of τ_f^* distribution at different moments.

5. Conclusions

In this paper, a new flow simulation method of fresh concrete was studied on the basis of SPH approach. The VGM model was employed as constitutive model, which can describe the nonlinear, shearing time-dependent, and pressure-dependent characteristics of the flow

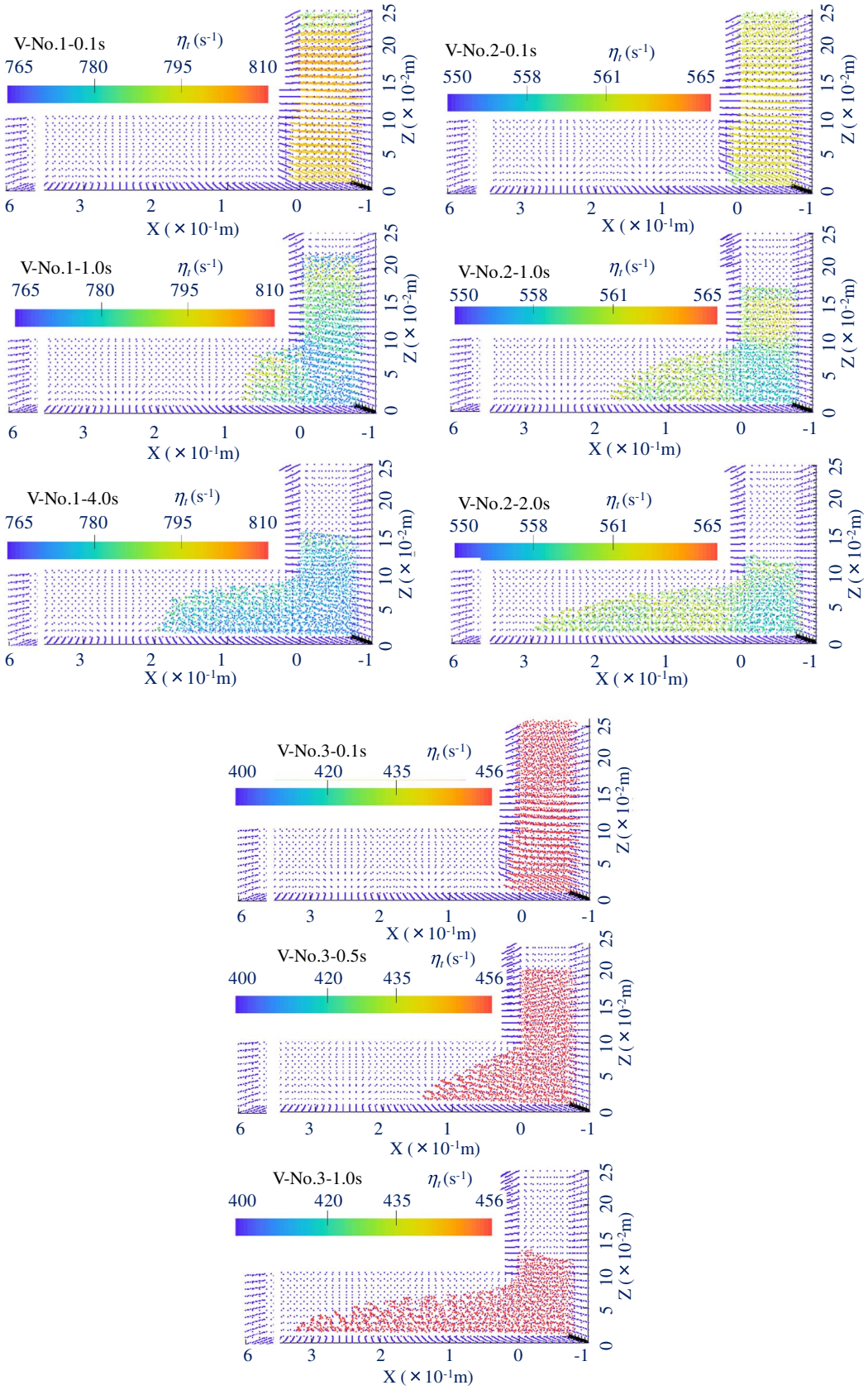

Fig. 11. Calculating results of η_f distribution at different moments.

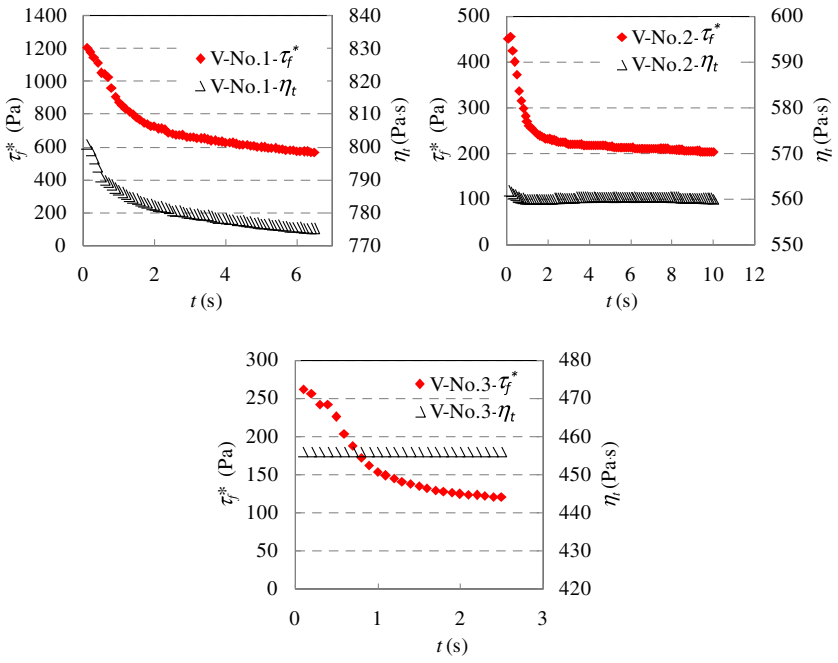

Fig. 12. Variations of τ_f^* and η_t in the VGM model with the flow time.

behaviors of fresh concrete. Moreover, a visco-plastic model was incorporated into the SPH approach for describing the slippage resistance of fresh concrete at the boundary. Then, the L-flow tests of three fresh mortar mixtures were performed to verify the validity of the proposed numerical method. And for making a comparison, the numerical flow simulations with the Bingham model were also conducted.

Fresh concrete has granular characteristic, including inter-particle friction, dilatant deformation, and particles' interlocking, etc. The degree of particles' interlocking is usually described by mean particle contact angle (θ). For the mixture with low fluidity, the particle contacts increase, and its granular characteristics are obvious. The mean inter-particle frictional angle (ϕ) and the normal stress (σ_n) on the shear plane are taken into account in the VGM model, by which the granular characteristics of fresh concrete are reflected. Moreover, The VGM model can reflect the flow behaviors affected by the change of θ with shear deformation. Therefore, the numerical results using the VGM model are more consistent with the experimental results than Bingham model. Also, the numerical simulation using the VGM model can reflect the shearing time-dependence of the flow behaviors since the yield stress and viscosity in the VGM model change with the shear flow.

However, for the mixture with high fluidity, its granular characteristic is not obvious, and the particles' interlocking has a little effect on its flow behaviors. Hence, the flow behaviors can be approximately described by Bingham model. Using the VGM model and the Bingham model got close numerical results.

Moreover, combining the VGM model and the visco-plastic model can increase the accuracy of SPH analysis of fresh concrete, especially for low fluidity concrete.

References

[1] C.F. Ferraris, F. de Larrard, Modified slump test to measure rheological parameters of fresh concrete, Cement, Concrete and Aggregates 20 (2) (1998) 241–247.
[2] C.F. Ferraris, Measurement of the rheological properties of high performance concrete: state of the art report, J. Res. Natl. Inst. Stand. Technol. 104 (5) (1999) 461.
[3] Z. Li, State of workability design technology for fresh concrete in Japan, Cem. Concr. Res. 37 (9) (2007) 1308–1320.
[4] R. Deeb, S. Kulasegaram, B. Karihaloo, 3D modelling of the flow of self-compacting concrete with or without steel fibres. Part I: slump flow test, Computational Particle Mechanics 1 (4) (2014) 373–389.
[5] H. Lashkarbolouk, A.M. Halabian, M.R. Chamani, Simulation of concrete flow in V-funnel test and the proper range of viscosity and yield stress for SCC, Mater. Struct. 47 (10) (2014) 1729–1743.
[6] Z. Li, T. Ohkubo, Y. Tanigawa, Flow performance of high-fluidity concrete, J. Mater. Civ. Eng. 16 (6) (2004) 588–596.
[7] Z. Li, T. Ohkubo, Y. Tanigawa, Yield model of high fluidity concrete in fresh state, J. Mater. Civ. Eng. 16 (3) (2004) 195–201.
[8] H. Mori, M. Tanaka, Y. Tanigawa, Experimental study on shear deformational behavior of fresh concrete, Journal of Structural and Construction Engineering 427 (1991) 1–10.
[9] Z. Li, J. Li, Granular material characteristic of fresh concrete, Proceedings of 6th International RILEM Symposium on Self-Compacting Concrete, 2010, pp. 423–433.
[10] J. Li, Z. Li, Effect of boundary restraint on the flow of fresh concrete through opening, Journal of Structure and Construction Engineering, Transaction of Archcitectural Instistue of Japan 76 (666) (2011) 1367–1374.
[11] J.E. Wallevik, Rheology of particle suspensions-fresh concrete, Ph. D Thesis of Norwegian University of Science and Technology, 2003, pp. 11–47.
[12] Z. Li, T. Ohkubo, Y. Tanigawa, Theoretical analysis of time-dependence and thixotropy of fluidity for high fluidity concrete, J. Mater. Civ. Eng. 16 (3) (2004) 247–256.
[13] N. Roussel, A thixotropy model for fresh fluid concretes: theory, validation and applications, Cem. Concr. Res. 36 (10) (2006) 1797–1806.
[14] A. Papo, Rheological models for cement pastes, Mater. Struct. 21 (1) (1988) 41–46.
[15] F. de Larrard, C.F. Ferraris, T. Sedran, Fresh concrete: a Herschel-Bulkley material, Mater. Struct. 31 (7) (1998) 494–498.
[16] D. Feys, R. Verhoeven, G. De Schutter, Steady-state rheological properties of fresh Self Compacting Concrete and their evolution in time, Annual Transactions the Nordic Rheology Society (2007) 35–41.
[17] H.H. Bui, R. Fukagawa, K. Sako, et al., Lagrangian meshfree particles method (SPH) for large deformation and failure flows of geomaterial using elastic–plastic soil constitutive model, Int. J. Numer. Anal. Methods Geomech. 32 (12) (2008) 1537–1570.
[18] S. Shao, E.Y. Lo, Incompressible SPH method for simulating Newtonian and non-Newtonian flows with a free surface, Adv. Water Resour. 26 (7) (2003) 787–800.
[19] F. Badry, S. Kulasegaram, B.L. Karihaloo, Estimation of the yield stress and distribution of large aggregates from slump flow test of self-compacting concrete mixes using smooth particle hydrodynamics simulation, Journal of Sustainable Cement-Based Materials 5 (3) (2016) 117–134.
[20] S. Kulasegaram, B.L. Karihaloo, Fibre-reinforced, self-compacting concrete flow modelled by smooth particle hydrodynamics, Proceedings of the Institution of Civil Engineers-Engineering and Computational Mechanics 166 (1) (2013) 22–31.
[21] Z. Li, Rheological model and rheometer of fresh concrete, Journal of Structural and Construction Engineering, Transaction of Archcitectural Instistue of Japan 80 (710) (2015) 527–537.
[22] M.B. Liu, G.R. Liu, Smoothed particle hydrodynamics (SPH): an overview and recent developments, Arch. Comput. Meth. Eng. 17 (1) (2010) 25–76.
[23] F.A. Allahdadi, T.C. Carney, J.R. Hipp, et al., High strain Lagrangian hydrodynamics: a three dimensional SPH code for dynamic material response, J. Comput. Phys. 109 (1) (1993) 67–75.
[24] G.R. Johnson, R.A. Stryk, S.R. Beissel, SPH for high velocity impact computations, Comput. Methods Appl. Mech. Eng. 139 (1–4) (1996) 347–373.
[25] M.B. Liu, G.R. Liu, Z. Zong, et al., Computer simulation of high explosive explosion using smoothed particle hydrodynamics methodology, Comput. Fluids 32 (3) (2003) 305–322.
[26] M.S. Shadloo, A. Zainali, M. Yildiz, et al., A robust weakly compressible SPH method and its comparison with an incompressible SPH, Int. J. Numer. Methods

Eng. 89 (8) (2012) 939–956.
[27] J.J. Monaghan, A. Kos, Solitary waves on a Cretan beach, J. Waterw. Port Coast. Ocean Eng. 125 (3) (1999) 145–155.
[28] J.J. Monaghan, Simulating free surface flows with SPH, J. Comput. Phys. 110 (2) (1994) 399–406.
[29] T.C. Papanastasiou, Flows of materials with yield, J. Rheol. 31 (5) (1987) 385–404.
[30] H. Zhu, N.S. Martys, C. Ferraris, et al., A numerical study of the flow of Bingham-like fluids in two-dimensional vane and cylinder rheometers using a smoothed particle hydrodynamics (SPH) based method, J. Non-Newtonian Fluid Mech. 165 (7) (2010) 362–375.
[31] Z. Li, Theoretical investigation on rheological properties of fresh concrete, Journal of Structural and Construction Engineering, Transaction of Archcitectural Institue of Japan 78 (687) (2013) 895–904.
[32] Z. Li, K. Kajiwara, M. Iidaka, Investigation on particle contact angle of fresh concrete using X-ray CT imaging, J. Soc. Mater. Sci., Jpn. 62 (9) (2013) 585–591.
[33] Z. Li, Y. Tanigawa, Investigation on granular characteristics of fresh concrete based on visualized experiment using alternative materials, Journal of Structural and Construction Engineering, Transaction of Archcitectural Institue of Japan 77 (678) (2012) 1175–1184.
[34] Z. Li, J. Li, Exterimental investigation on shear defromation of fresh concrete, Journal of Structural and Construction Engineering, Transaction of Archcitectural Institue of Japan 75 (653) (2010) 1173–1180.
[35] Y. Sakihara, S. Iraha, T. Iribu, et al., Numerical flow simulation of fresh concrete with SPH, Japan Concrete Institute 26 (1) (2004) 1149–1154.
[36] J. Murata, K. Suzuki, Study on grout flow in pipe with slip at wall, Proc. Jpn Soc. Civ. Eng. 38 (7) (1987) 129–136.
[37] J.J. Monaghan, On the problem of penetration in particle methods, J. Comput. Phys. 82 (1) (1989) 1–15.